Supporting Information for

Flexible 2D Crystals of Polycyclic Aromatics Stabilized by Static Distortion Waves

Matthias Meissner,[1] Falko Sojka,[1] Lars Matthes,[2] Friedhelm Bechstedt,[2] Xinliang Feng,[3†] Klaus Müllen,[3] Stefan C. B. Mannsfeld,[4] Roman Forker,[1] Torsten Fritz[1,5]

[1]Institute of Solid State Physics, Friedrich Schiller University, Helmholtzweg 5, 07743 Jena, Germany

[2]Institute of Condensed Matter Theory and Solid State Optics, Friedrich Schiller University, Fröbelstieg 1, 07743 Jena, Germany

[3]Max Planck Institute for Polymer Research, Ackermannweg 10, 55128 Mainz, Germany

[4]Center for Advancing Electronics, University of Technology Dresden, Würzburger Str. 46, 01187 Dresden, Germany

[5]Graduate School of Science and Institute for Academic Initiatives, Department of Chemistry, Osaka University, 1-1 Machikaneyama, Toyonaka 560-0043, Osaka, Japan

[†]present address: Center for Advancing Electronics Dresden & Department of Chemistry and Food Chemistry, University of Technology Dresden, Mommsenstrasse 4, 01062 Dresden, Germany

Content

1. HBC on Natural Graphite

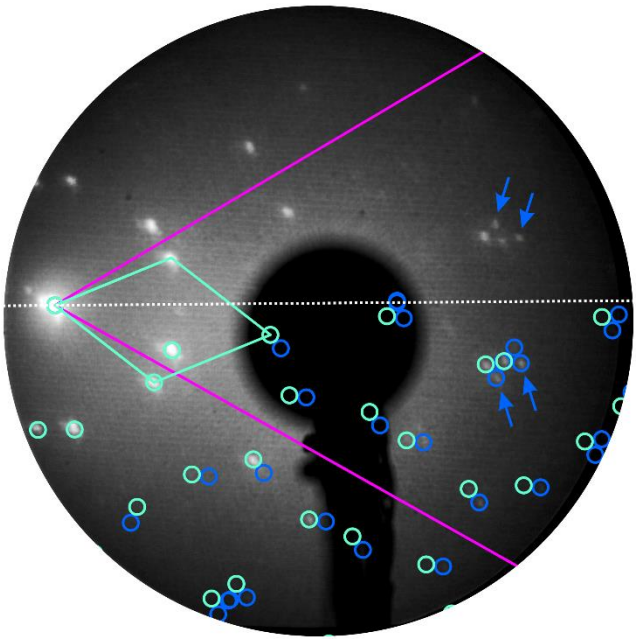

Supplementary Figure 1. *Room temperature LEED image (incident electron energy 25.2 eV, sample tilted by 15°, logarithmic contrast) of 1 HBC monolayer on natural graphite (NG), corrected for imaging and tilt distortions. The magenta lines originating from the specular spot correspond to the directions of the first order substrate spots, hence, the sample is azimuthally rotated by roughly 30° with respect to the sample in Fig. 1a of the main paper. Turquoise circles mark spots due to the HBC lattice. Spots consistent with multiple scattering between the HBC and graphite lattices (blue circles) are necessary to explain all spots. Blue arrows mark the most intense multiple scattering spots – the same ones as marked in Fig. 1a of the main paper. Their identical positions relative to HBC spots confirm an equivalent incommensurate epitaxy of HBC on epitaxial graphene and NG.*

2. Determining the Molecular Orientation

Thanks to the high resolution of the STM images we can determine the molecular orientation angles β with respect to the HBC lattice vector and α with respect to the substrate lattice vector (cf. Fig. 1c in the main paper). For this, the STM image in Fig. 1b in the main paper and an additional STM image of the equivalent mirror domain (not shown) were corrected for shear distortions. Then, circular line profiles cutting through the outmost benzene rings of all fully imaged molecules – 12 and 13, respectively – were extracted using ImageJ[1] with the Oval Profile Plot plugin.

Supplementary Fig. 2a shows the corresponding curves and their average. From the latter the angular positions of the 12 nodes (minima on the profile) were obtained. Due to the molecular symmetry the nodes must be separated by 30°, and thus their angular positions can be fitted linearly. Together with the shape of the calculated HOMO (cf. Fig. 1c in the main paper) this gives the best possible estimate of the orientation of the molecules. In relation to the orientation of the HBC lattice vector $\boldsymbol{a}_1$ this results in $\beta = (5.1 \pm 0.5)°$.

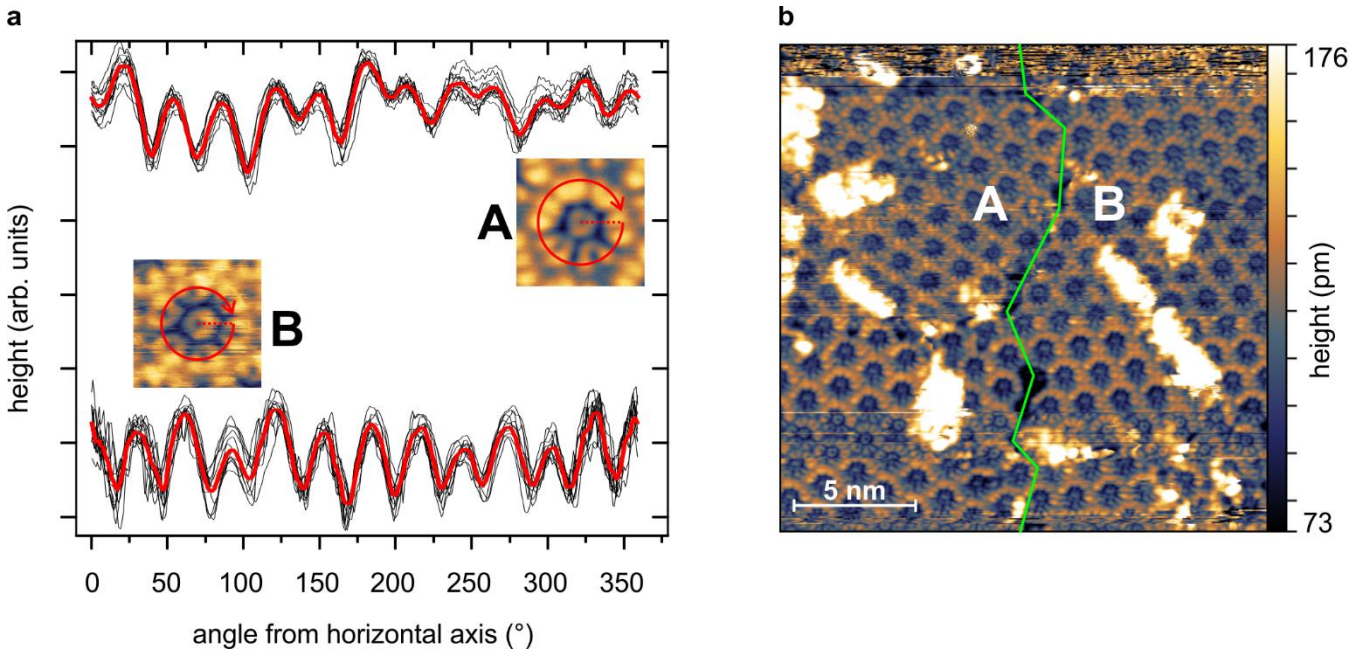

Supplementary Figure 2. a, *Angular profiles (black) and their averages (red) around the 12 molecules in Fig. 1b of the main paper (top curve; domain A) and 13 molecules in an additional image of the mirror domain (bottom curve; domain B).* ***b,*** *STM image taken at 4.4 K with a sample bias of -3 V and a setpoint of 3 pA, displaying the boundary between the two possible mirror domains, one on the left half, one on the right half of the image.*

Further, Supplementary Fig. 2b shows an area where the two possible mirror domains meet (rotationally equivalent domains are identical to each other here). With the help of this image, even though of slightly reduced quality, the angle between the HBC molecules and the substrate can be unambiguously determined: Since the angle $\theta = -8.66°$ between the HBC lattice vector $\boldsymbol{a}_1$ and the substrate lattice vector $\boldsymbol{s}_1$ is known from LEED there is only one possible orientation of $\boldsymbol{s}_1$ that encloses the angle θ with $\boldsymbol{a}_1$ of both mirror domains, determining the molecular angle α = (-3.6 ± 0.5)° with respect to $\boldsymbol{s}_1$.

3. Moiré Pattern in Real and Reciprocal Space

A Moiré pattern in STM images in form of a brightness modulation (Supplementary Fig. 3a) can have different origins. Owing to differing adsorption sites of the adsorbate it can either be a merely electronic effect or a real adsorption height modulation. In both cases, the modulation is driven by the structure of the substrate, and the apparent shape of the Moiré pattern is the result of "mixing" the substrate and adsorbate lattices. Specifically, it has been shown that modulated crystals produce the same geometric features in diffraction experiments as multiple scattering effects, i.e., a geometric convolution of the two reciprocal lattices.[2,3] Note that this is not limited to a height modulation, but that a modulation of the lateral coordinates of the adsorbate will yield the same geometric convolution.

Consequently, a Fast Fourier Transform (FFT) of an STM image can be treated much like a LEED pattern exhibiting multiple scattering spots. Each additional frequency due to the Moiré pattern can be thought of as originating from both a substrate and an adsorbate lattice point. Hence, the relation between the two lattices, i.e., the epitaxy matrix, can be determined from the pattern using LEEDLab (from Scienta Omicron) without directly observing the (in this case) relatively high frequencies of the substrate lattice.

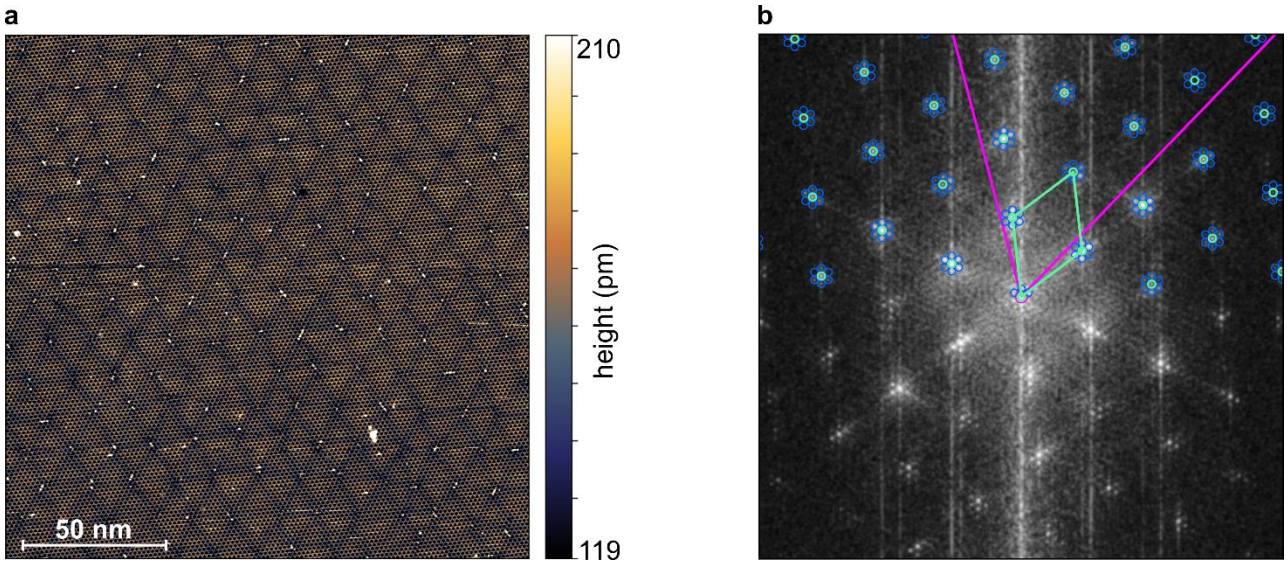

Supplementary Figure 3. a, *180 x 180 nm^2 STM image taken at 1.2 K with a sample bias of +3 V and a setpoint of 2 pA, displaying a single HBC domain which even extends far beyond this image in the µm range, and a Moiré contrast. Although disturbed by defects, the average long-range order is obvious and reflected in the Fast Fourier Transform in panel* ***b,*** *which shows sharp modulation frequencies (blue circles) around the HBC reciprocal lattice spots (turquoise circles). The direction of the substrate lattice vectors (magenta lines) is obtained via the inverse of the epitaxy matrix determined with LEED.*

One peculiarity in such an analysis of an STM FFT is that generally any STM image is distorted to some degree owing to drift effects, the non-linearity of the scanner in large scan ranges or simply an imperfect piezo calibration. At the low temperatures applied here the distortion is linear (i.e., shear and/or scaling) around the image center in good approximation. In our case, the HBC lattice is sheared from its exactly hexagonal shape in any STM image which, of course, translates into the FFT, too. However, linear distortions, i.e., distortions that can

be expressed with a single transformation matrix, do not affect the epitaxy matrix because substrate and adsorbate are identically distorted in a given STM image. Hence, if the epitaxy relation is determined in a sheared image it can directly be applied to the known (non-sheared) substrate lattice to give the true non-sheared adsorbate lattice.

The FFT in Supplementary Fig. 3b can be analyzed accordingly. First, using LEEDLab, the (sheared) HBC lattice is determined directly via the HBC spots. Second, in a reverse fashion, applying the inverse of the epitaxy matrix from LEED measurements to the HBC structure gives an estimate for where the (sheared) substrate lattice would be expected in the FFT. In this case, the frequencies – if observable at all – would lie outside the accessible range. However, the substrate-induced satellite spots around the HBC spots contain the indirect information about the substrate lattice. Thus, with the multiple scattering function of LEEDLab the estimated position of the satellite spots can be calculated and the spots can be identified accordingly. In the discussed case this works very well since the difference between the room temperature structure measured with LEED and the low temperature structure in the STM is very small. Finally, a fit routine optimizes both the epitaxy matrix and the adsorbate lattice, effectively allowing both (sheared) lattices to vary freely. The resulting epitaxy matrix $\begin{pmatrix} 5.113(5) & -0.986(1) \\ 0.985(1) & 6.092(6) \end{pmatrix}$ can be applied to the theoretical non-sheared substrate to obtain the lattice parameters given Table 1 in the paper. A possible temperature-dependent change in the graphite lattice constant is not considered here since the HBC lattice constant is only presented for the sake of completeness. The epitaxy matrix contains all necessary information to account for a change in the substrate lattice constant.

4. Nearest-Neighbor Distance Distributions

Molecular positions in the STM image of Fig. 2a of the main paper were measured by applying an algorithm that was originally developed to identify spot positions in LEED patterns. In this algorithm, the intensity maxima are determined with sub-pixel resolution by fitting them with Gaussian intensity distributions.[4] Since in the image the molecules' centers appear dark, we used contrast-reversed images for this procedure.

In order to achieve the best result we took care to minimize the effect of the non-linearity of the piezo scanner by cropping 50% of the STM image height and width, as the center is least influenced by this effect. Since we know from LEED and the Fourier analysis of the Moiré pattern that the HBC layer is hexagonal we can correct the images for any left-over linear distortions. This is mandatory in order to correctly measure the magnitude of the displacements given in the main paper and the distribution of nearest-neighbor distances.

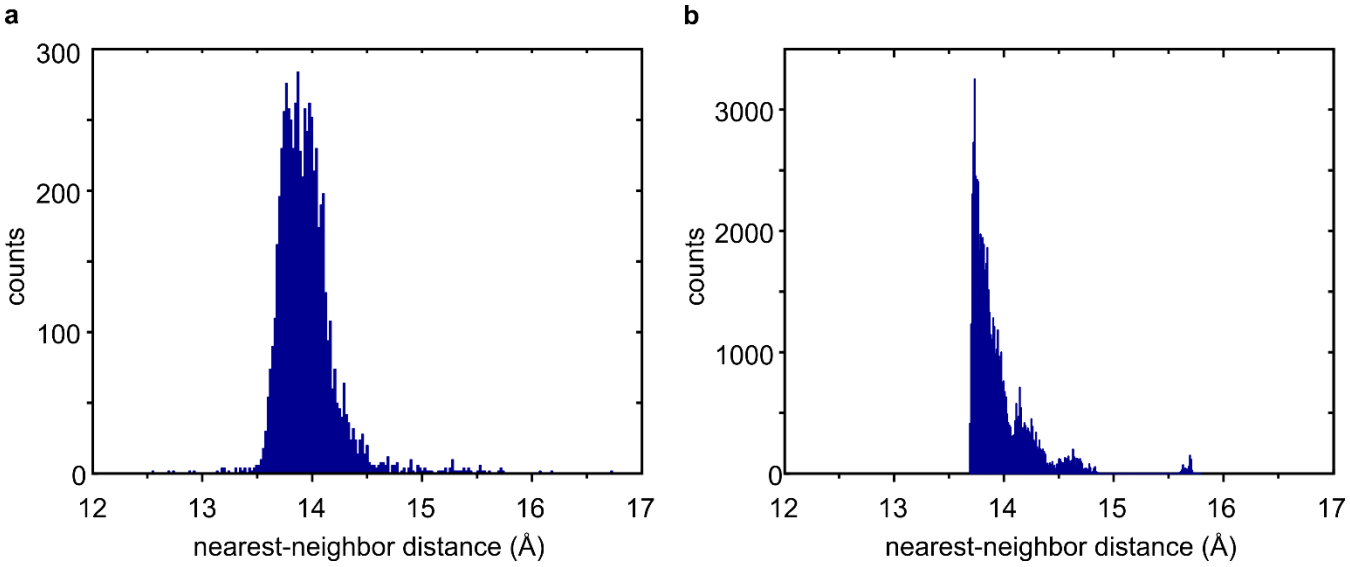

Supplementary Figure 4. a, *Experimental distribution of nearest-neighbor distances extracted from the STM image in Fig. 2a in the main paper.* ***b,*** *Corresponding calculated distribution from the relaxed HBC domain of Figs. 2c and 2d of the main paper.*

Supplementary Fig. 4a displays the measured distribution of nearest-neighbor distances, while Supplementary Fig. 4b shows such a distribution numerically obtained from the relaxed low-temperature overlayer described in the main paper and illustrated there in Fig. 2. Both graphs have very similar shapes. The mean distance is the same because the experimental mean distance was the starting configuration for the numerical relaxation. However, the measured distribution is obviously broadened due to defects and statistical errors of the localization algorithm, while the theoretical distribution has a sharp cutoff towards distances smaller than 13.7 Å. Though this constitutes the "commensurate" value from the literature, no extended areas of a commensurate phase, as reported by others,[5] were detectable in STM or in LEED. Due to the quasi-static relaxation algorithm the molecules will simply not get closer because there is no such force once they reach the "commensurate" distance.

5. Comparison of Force-Field and DFT Calculations

Supplementary Fig. 5a shows the force-field map $E_{\mathrm{mol-sub}}(\boldsymbol{r}, \alpha = 0°)$ over one graphite unit cell which contains both the highest and lowest possible values of $E_{\mathrm{mol-sub}}$ for an HBC molecule on graphite. It has been offset and scaled to match DFT calculations of the AB (bernal) and AA stacking of an HBC molecule on graphite. Additional DFT values along the marked line show that the scaled map represents the DFT energy landscape very well (cf. Supplementary Fig. 5b). If the same scaling is applied to maps of different orientation angles α the agreement is reasonable as well, including an almost disappearing maximum energy difference for $\alpha \approx 12°$.

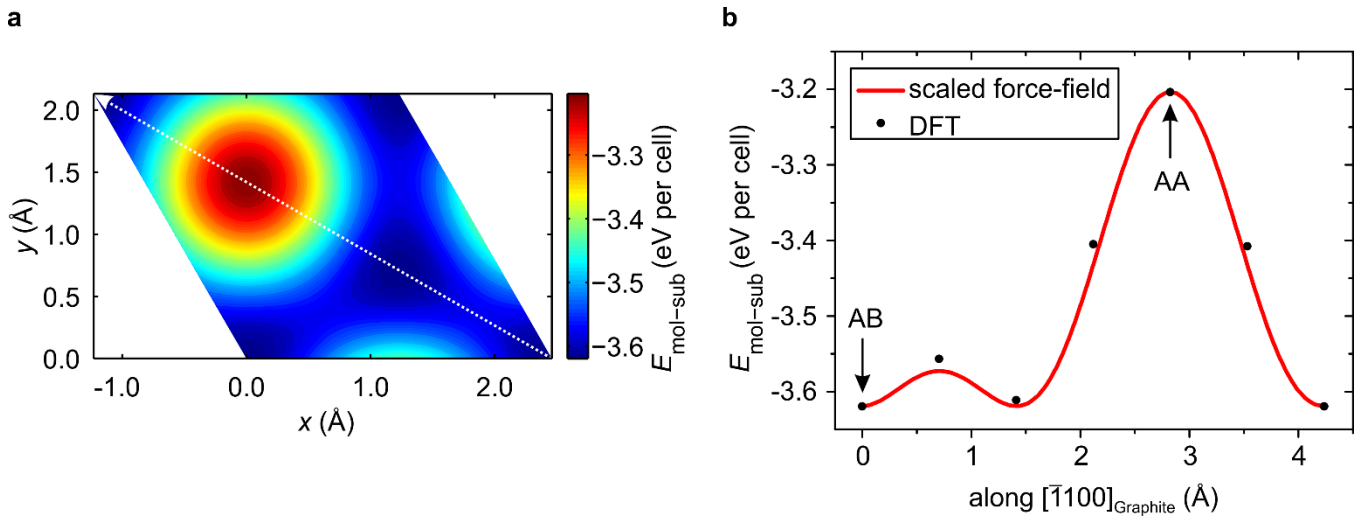

Supplementary Figure 5. a, *$E_{mol-sub}(r, \alpha = 0°)$ map over one graphite unit cell, offset and scaled to match the lowest and highest DFT energy configurations (HBC in AB and AA stacking, respectively). Along the white line a profile is extracted and plotted in* ***b,*** *where it can be compared to additional DFT calculations along the same line, which show a reasonable agreement.*

6. Parametrization of DFT Calculations

The mechanism of the relaxation algorithm is to determine the local gradient of the total energy $E_{\mathrm{mol-sub}} + E_{\mathrm{mol-mol}}$ with respect to a molecular displacement $\boldsymbol{\delta}_p$ and then to adjust $\boldsymbol{\delta}_p$ accordingly. The gradient of $E_{\mathrm{mol-sub}}$ is obtained in a straightforward way from the $E_{\mathrm{mol-sub}}$ maps depending on the orientation of the molecule. Due to the high resolution the maps can be interpolated, if needed. The gradient of $E_{\mathrm{mol-mol}}$ is more challenging. The extended shape of the HBC molecule with its attached hydrogens makes the intermolecular interaction strongly anisotropic. Hence, we split it into two contributions: a longitudinal deformation of a bond between two neighboring molecules parallel to the bond ($E_{\mathrm{mol-mol},||}$) and a shear deformation perpendicular to the bond direction ($E_{\mathrm{mol-mol},\perp}$). Both can be obtained via DFT. Since in a 2-dimensional hexagonal lattice there are three times as many nearest neighbor bonds as there are lattice points, all DFT energies are divided by a factor of 3, condensing all energetic change into one nearest-neighbor bond deformation.

The calculated equilibrium configuration of a free-standing HBC layer is determined to be a hexagonal cell with a lattice constant of $a_0 = 14.15$ Å and a molecular angle of $\beta_0 = 6°$. The overestimation of both values compared to the experimental ones (13.95 Å and 5.1°, respectively) is in a reasonable range so that we can apply a rigid shift to the following DFT energy curves in order to match the experimental equilibrium configuration without large errors.

We calculate the longitudinal contribution by simply stretching and compressing the HBC unit cell. Supplementary Fig. 6a shows the resulting energy curve as a function of the lattice constant a. It can be fitted by a Mie potential of the shape $E_{\mathrm{mol-mol},||} = \left(\frac{c_1}{a}\right)^m - \left(\frac{c_2}{a}\right)^n$ (for fit result see Table S1). To match the experimental equilibrium distance a shift of $\Delta a = 0.2$ Å is applied: $E_{\mathrm{mol-mol},||} = \left(\frac{c_1}{a+\Delta a}\right)^m - \left(\frac{c_2}{a+\Delta a}\right)^n$.

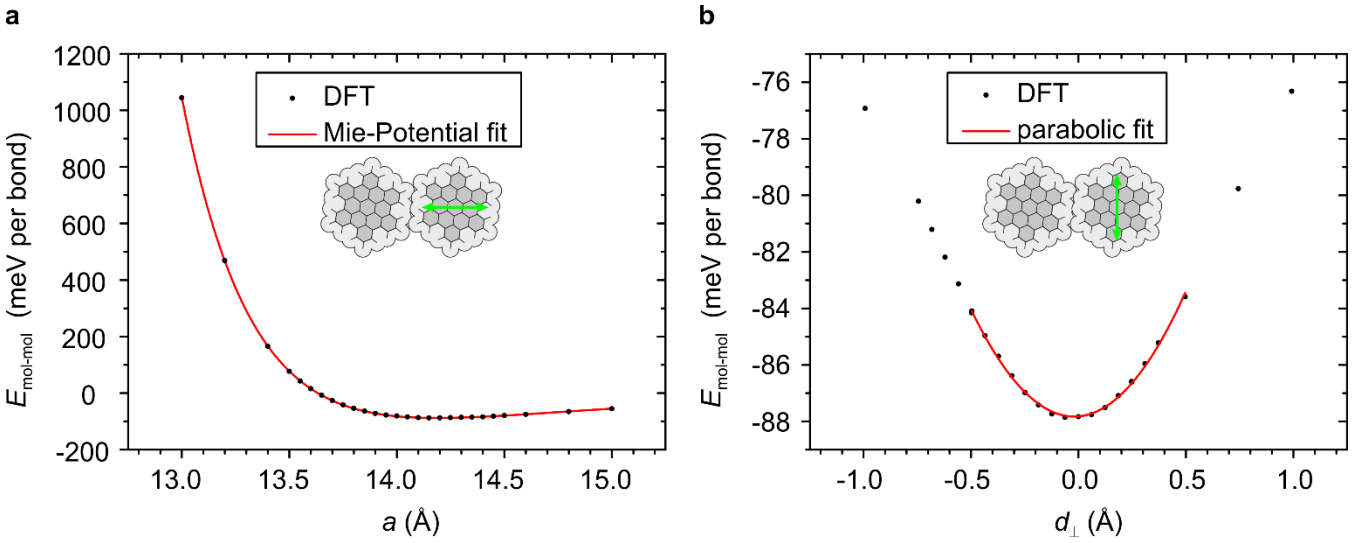

Supplementary Figure 6. a, *DFT energy for a longitudinal deformation of an intermolecular nearest-neighbor bond and the fitted Mie potential.* ***b,*** *DFT energy for a shear deformation of an intermolecular nearest-neighbor bond and the fitted parabola. Both minima correspond to the DFT equilibrium configuration ($a_0 = 14.15$ Å and $\beta_0 = 6°$).*

Now we consider a molecule p, displaced from its lattice point $\boldsymbol{r}_p$ by $\boldsymbol{\delta}_p$, and a nearest neighbor q, displaced by $\boldsymbol{\delta}_q$ from $\boldsymbol{r}_q$. The projected longitudinal displacement $\delta_{||,pq} = (\boldsymbol{\delta}_p - \boldsymbol{\delta}_q) \cdot (\boldsymbol{r}_p - \boldsymbol{r}_q)/|(\boldsymbol{r}_p - \boldsymbol{r}_q)|$ then changes the energy as follows: $E_{\mathrm{mol-mol},||}(\boldsymbol{\delta}_p, \boldsymbol{\delta}_q) = \left(\frac{c_1}{a+\Delta a+\delta_{||,pq}}\right)^m - \left(\frac{c_2}{a+\Delta a+\delta_{||,pq}}\right)^n$. Note that here the binding energy of the two binding molecules (minimum of $E_{\mathrm{mol-mol},||}$) is already fully included.

To obtain the shear contribution due to a perpendicular displacement $\delta_{\perp,pq} = \sqrt{(\boldsymbol{\delta}_p - \boldsymbol{\delta}_q)^2 - \delta_{||,pq}^2}$ we vary the HBC cell size according to $a = \sqrt{a_0^2 + \delta_\perp^2}$ while changing the molecular angle within the unit cell $\beta = \beta_0 + \arctan(\delta_\perp/a_0)$. The result is plotted in Supplementary Fig. 6b. It can be fitted satisfactorily by a parabola $E_{\mathrm{mol-mol},\perp} = E_0 + c_3{\delta_\perp}^2$ (cf. Supplementary Table 1). However, since a shear of the bond should only provide an additional increase in $E_{\mathrm{mol-mol}}$ while leaving the equilibrium energy unchanged only the curvature term is needed.

Supplementary Table 1 | Fit parameters. *The fit parameters given here describe $E_{mol-mol}$ in meV.*

c_1	c_2	m	n	c_3
16.01 ± 0.02	19.32 ± 0.05	35.8 ± 0.2	16.5 ± 0.2	16.4 ± 0.2

With this, the interaction energy of one intermolecular bond is

$$E_{\mathrm{mol-mol}} = \left(\frac{c_1}{a + \Delta a + \delta_{||,pq}}\right)^m - \left(\frac{c_2}{a + \Delta a + \delta_{||,pq}}\right)^n + c_3{\delta_{\perp,pq}}^2.$$

Finally, the total energy of a molecular domain of N molecules can thus be calculated by summation based on the displacements of each molecule and the displacements of its nearest neighbors:

$$E_{\mathrm{total}} = \sum_{p=1}^{N}\left[E_{\mathrm{mol-sub}}(\boldsymbol{r}_p + \boldsymbol{\delta}_p, \alpha) + \frac{1}{2}\sum_q E_{\mathrm{mol-mol}}(\boldsymbol{\delta}_p, \boldsymbol{\delta}_q)\right].$$

The factor ½ stems from the fact that we sum over all molecules, not all bonds (i.e., pairs of molecules). Hence, each bond appears twice which needs to be accounted for.

The advantage of the above parametrization is the ability to analytically calculate the gradient of the total energy with respect to the displacement of the p^{th} molecule $\frac{\partial}{\partial \boldsymbol{\delta}_p} E_{\mathrm{total}} = \boldsymbol{\nabla}_p E_{\mathrm{mol-sub}} + \boldsymbol{\nabla}_p E_{\mathrm{mol-mol}}$ from the parametrized energy curves:

$$\boldsymbol{\nabla}_p E_{\mathrm{total}} = \boldsymbol{\nabla}_p E_{\mathrm{mol-sub}} + \left[-\frac{m\, c_1^m}{(a + \Delta a + \delta_{pq,\parallel})^{m+1}} + \frac{n\, c_2^n}{(a + \Delta a + \delta_{pq,\parallel})^{n+1}}\right]\hat{\boldsymbol{r}}_{pq} + 2c_3\delta_{pq,\perp}\hat{\boldsymbol{r}}_{pq,\perp}$$

with $\hat{\boldsymbol{r}}_{pq}$ being the unit vector in the direction $\boldsymbol{r}_p - \boldsymbol{r}_q$ and $\hat{\boldsymbol{r}}_{pq,\perp}$ the respective unit vector perpendicular to $\hat{\boldsymbol{r}}_{pq}$. Note that the factor of ½ is canceled here again since each gradient $\boldsymbol{\nabla}_p E_{\mathrm{mol-mol}}(\boldsymbol{\delta}_p, \boldsymbol{\delta}_q)$, along with each bond, appears twice in the total sum.

7. Non-Relaxed *Versus* Relaxed Moiré Patterns

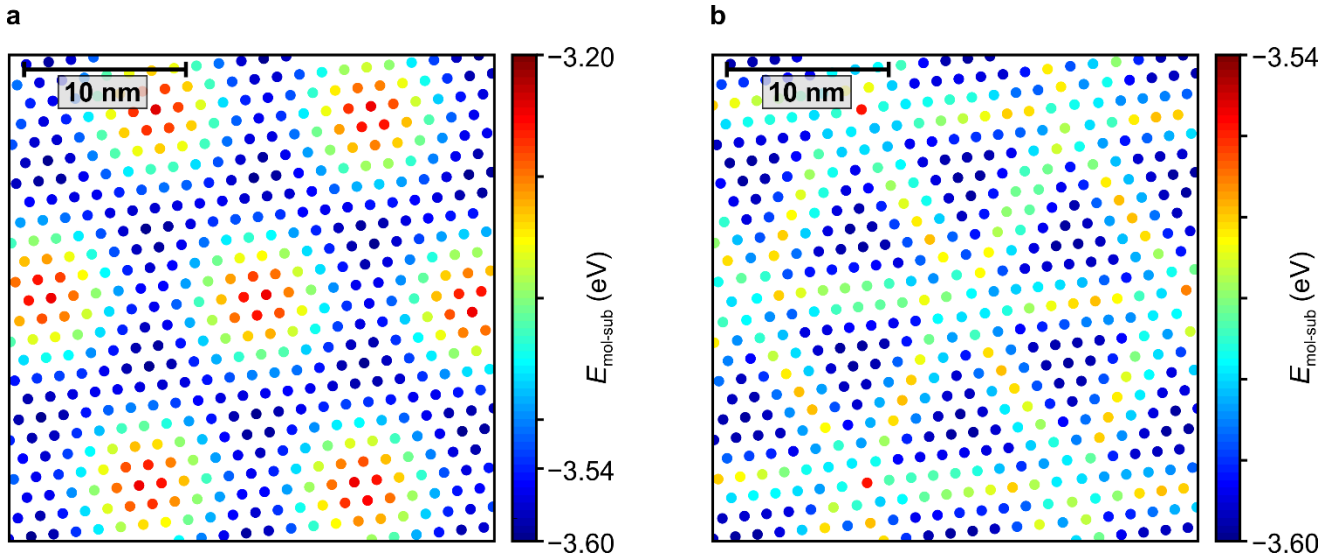

Supplementary Figure 7. a, *Hexagonal unrelaxed HBC lattice with the experimental low-temperature lattice constant and unit cell orientation. The molecule-substrate interaction energy* $E_{mol-sub}$ *at the respective molecular positions is color-coded.* ***b,*** *HBC positions after the relaxation of the domain in panel a) and the corresponding energies* $E_{mol-sub}$ *(reproduced from Fig. 2c of the main paper for comparison). Only the relaxed structure matches the experimental Moiré pattern in Fig. 2a of the main paper. The decreased range of* $E_{mol-sub}$ *that covers only the lower part of the range in panel* ***a*** *illustrates the gain in molecule-substrate energy due to the relaxation.*

8. Domain Size Dependence and Relaxation of Room Temperature Structure

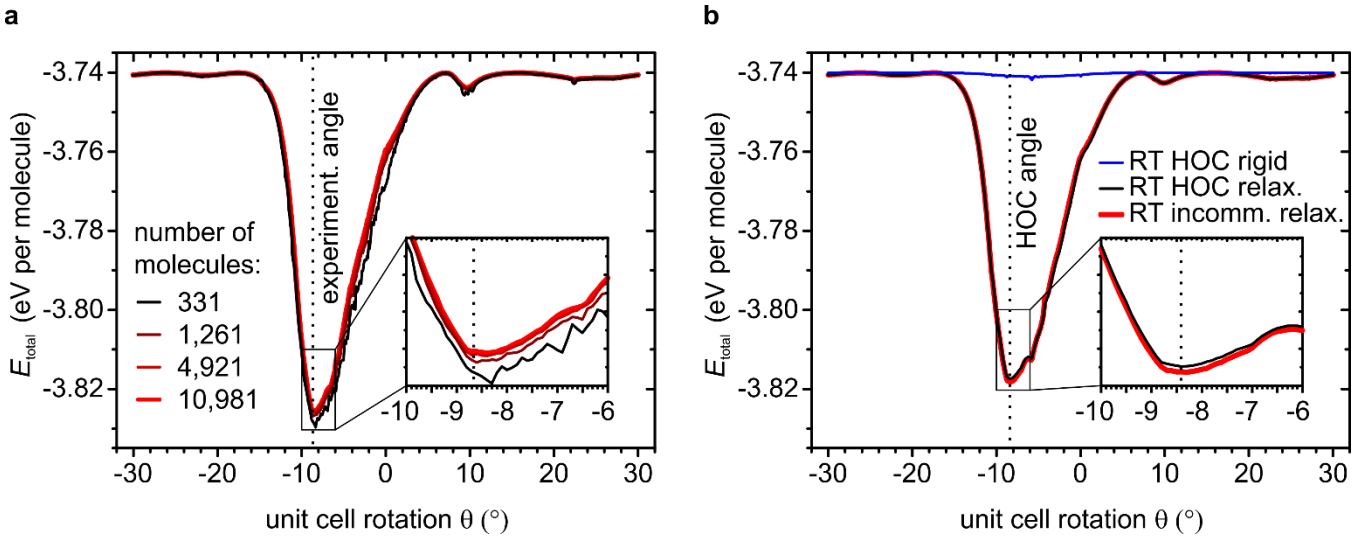

Supplementary Figure 8. a, *Total adsorption energy per molecule after relaxation of HBC domains with different sizes, initially separated by the experimental LT lattice constant of 13.95 Å. For better comparison, small offsets (decreasing with increasing domain size) due to molecules with fewer than 6 nearest neighbors at domain edges have been corrected for the three smaller domains, using the values -14 meV, -6 meV, and -1 meV. Obviously, with increasing domain size the minima are merely better defined due to the decreasing edge effects that result from the finite domain size. The experimental LT angle θ = -8.66° is marked by a dotted line.* ***b,*** *Total adsorption energy per molecule of HBC domains with 10,981 molecules, before (blue line) and after (black line) relaxation, initially separated by a lattice constant of 14.0174 Å that produces an HOC coincidence at θ = -8.41° (marked by dotted vertical line), which is similar but not identical to the measured incommensurate room-temperature (RT) structure. For comparison, the corresponding curve of the relaxed incommensurate RT structure plotted in red.*

Supplementary References

(1) Schneider, C. A.; Rasband, W. S.; Eliceiri, K. W. NIH Image to ImageJ: 25 Years of Image Analysis. *Nat. Methods* **2012**, *9*, 671–675.

(2) Van Smaalen, S. *Incommensurate Crystallography*; IUCr monographs on crystallography; OUP Oxford, 2007.

(3) Van Hove, M. A.; Weinberg, W. H.; Chan, C.-M. *Low-Energy Electron Diffraction: Experiment, Theory and Surface Structure Determination*; Springer Series in Surface Sciences 6; Springer: Berlin, 1986.

(4) Sojka, F.; Meissner, M.; Zwick, C.; Forker, R.; Fritz, T. Determination and Correction of Distortions and Systematic Errors in Low-Energy Electron Diffraction. *Rev. Sci. Instrum.* **2013**, *84*, 015111.

(5) Woods, C. R.; Britnell, L.; Eckmann, A.; Ma, R. S.; Lu, J. C.; Guo, H. M.; Lin, X.; Yu, G. L.; Cao, Y.; Gorbachev, R. V.; Kretinin, A. V.; Park, J.; Ponomarenko, L. A.; Katsnelson, M. I.; Gornostyrev, Y. N.; Watanabe, K.; Taniguchi, T.; Casiraghi, C.; Gao, H.-J.; Geim, A. K. *et al*. Commensurate-Incommensurate Transition in Graphene on Hexagonal Boron Nitride. *Nat. Phys.* **2014**, *10*, 451–456.